Demonstrate chiral spin currents with nontrivial interactions in superconducting quantum circuit

Xiang-Min Yu(喻祥敏), Xiang Deng(邓翔), Jian-Wen Xu(徐建文), Wen Zheng(郑文), Dong Lan(兰栋), Jie Zhao(赵杰), Xinsheng Tan(谭新生), Shao-Xiong Li(李邵雄)[†], and Yang Yu(于扬)[‡]

National Laboratory of Solid State Microstructures, School of Physics, Nanjing University, Nanjing 210093, *China*

(Received 21 October 2022; revised manuscript received 30 November 2022; accepted manuscript online 16 December 2022)

Quantum many-body systems in which time-reversal symmetry is broken give rise to a wealth of exotic phases, and thus constitute one of the frontiers of modern condensed matter physics. Quantum simulation allows us to better understand many-body systems with huge Hilbert space, where classical simulation is usually inefficient. With superconducting quantum circuit as a platform for quantum simulation, we realize synthetic Abelian gauge fields by using microwave drive and tunable coupling in loop configurations to break the time-reversal symmetry of the system. Based on high-precision manipulation and readout of circuit-QED architecture, we demonstrate the chiral ground spin current of a time-reversal symmetry broken system with nontrivial interactions. Our work is a significant attempt to simulate quantum many-body systems with time-reversal symmetry breaking in multi-qubit superconducting processors.

Keywords: superconducting qubit, time-reversal symmetry breaking, chirality

PACS: 71.10.Fd, 42.50.Ct, 74.50.+r **DOI:** 10.1088/1674-1056/acac17

1. Introduction

Exploring new phase of matter is always the main topic of condensed matter physics. Quantum many-body systems composed of a large number of microscopic particles can generate rich and novel phases, especially when the time-reversal symmetry of the system is broken, such as fractional quantum Hall (FQH) phases where the magnetic field breaks the time-reversal symmetry of the two-dimensional electron-gas system.[1,2] Therefore, the study of time-reversal symmetry-breaking (TRSB) many-body systems is of profound importance. However, with the increase in degrees of freedom, the Hilbert space dimension grows exponentially, making it difficult to compute many-body systems with classical simulation techniques. As a result, Richard Feynman proposed the idea of quantum simulation, which transforms the challenging computational problem into an experimental problem involving the manipulation and measurement of controllable quantum systems.[3–5]

During the last few decades, a variety of physical platforms have been suggested as quantum simulators, such as ion traps,[6,7] cold atoms,[8] and neutral atoms.[9] Among these physical platforms, superconducting quantum circuits have advantages in terms of flexibility and scalability, especially, with longer coherence time and improved readout accuracy, and thus are one of the important candidates for building practical quantum simulators.[10–12] In a typical multiqubit superconducting circuit, each qubit is manipulated by two independent control lines, i.e., the X/Y control line and the Z control line, to achieve the X/Y direction and Z direction rotations.[13] Meanwhile, the qubits are connected to each other by tunable couplers to obtain the tunable XY-type coupling.[14–16] In the last decade, TRSB has already been demonstrated in superconducting quantum circuits,[17–20] where the time-reversal symmetry of the system was broken by the artificial gauge fields that were generated by gauge-invariant phases in closed loops, analogous to the Peierls phases accumulated in the external magnetic fields. Several techniques, such as Floquet engineering and the parametric modulation method, have been used to produce gauge-invariant phases in a triangular plaquette coupling geometry. Nevertheless, the previous research was mainly limited to the free fermion model which is fully solvable.

In this paper, we create nontrivial interactions by altering the coupling geometry between the superconducting qubits, and the exact dynamics evolution can be derived analytically in this physical model by exploiting the symmetry of the system. Unlike the prior methods, we realize the Abel gauge field using the phases of transverse fields rather than longitudinal fields to break the time-reversal symmetry of the system. We present a simple scheme to implement the physical model on a two-qubit superconducting quantum processor and experimentally observe the chiral spin current which is a consequence of time-reversal symmetry breaking. The scheme we proposed is experimentally easier to tune the gauge-invariant phase than a straightforward more qubits implementation.[18] Our work actually implements the simulation of the minimal model of a time-reversal symmetry broken system with non-trivial interaction and thus lays the groundwork for further research.

[†]Corresponding author. E-mail: shaoxiong.li@nju.edu.cn
[‡]Corresponding author. E-mail: yuyang@nju.edu.cn

© 2023 Chinese Physical Society and IOP Publishing Ltd

2. Physical model

The minimal physical model for the TRSB systems with non-trivial interaction is illustrated in Fig. 1(a). The coupling geometry of the four spin-1/2 particles consists of two triangular plaquettes, which share a common coupling. The coupling strength in each plaquette is complex-valued here, similar to the Peierls coupling in the presence of a magnetic field. Consequently, we treat the Hamiltonian of the spin system in a practical parameterization

$$\begin{aligned} H &= \sum_{\langle j,k\rangle} g_{jk}\left(\mathrm{e}^{\mathrm{i}\phi_{jk}}\sigma_j^{\dagger}\sigma_k + \mathrm{e}^{-\mathrm{i}\phi_{jk}}\sigma_j\sigma_k^{\dagger}\right) \\ &= g\left(\mathrm{e}^{\mathrm{i}\phi_{12}}\sigma_1^{\dagger}\sigma_2 + \mathrm{e}^{\mathrm{i}\phi_{31}}\sigma_3^{\dagger}\sigma_1 + \mathrm{e}^{\mathrm{i}\phi_{24}}\sigma_2^{\dagger}\sigma_4\right. \\ &\quad \left. + \mathrm{e}^{\mathrm{i}\phi_{43}}\sigma_4^{\dagger}\sigma_3 + \mathrm{e}^{\mathrm{i}\phi_{23}}\sigma_2^{\dagger}\sigma_3\right) + \mathrm{h.c.}, \end{aligned} \tag{1}$$

where the angle bracket indicates the nearest neighbor coupling, the operator σ_j ($\sigma_j^{\dagger}$) denotes the spin lowering (raising) Pauli operator of the particle j, and the coefficients g_{jk} and ϕ_{jk} indicate the magnitudes and static phases of the coupling strengths between particle j and particle k , respectively.

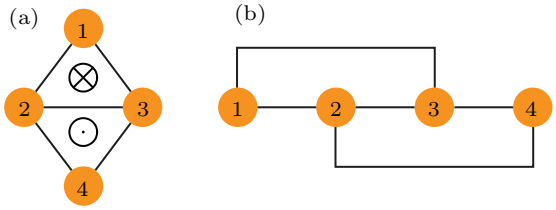


Fig. 1. The coupling geometry of the physical model. (a) Two triangular plaquettes with nearest-neighbor (NN) coupling. The complex-valued coupling strength can result in the local flux, which may cause TRSB. (b) Equivalent 1D spin chain with next nearest-neighbor (NNN) coupling.

At first glance, we notice that the sums of the phases in the loop configurations are gauge-invariant, especially for each triangular plaquette. In fact, let us consider a $U(1)$ gauge transformation, which is equivalent to $\sigma_j \to \tilde{\sigma}_j = \mathrm{e}^{-\mathrm{i}\phi_j}\sigma_j$. Thus, the Hamiltonian under the gauge transformation becomes

$$\begin{aligned} H &= g\left(\tilde{\sigma}_1^{\dagger}\tilde{\sigma}_2\,\mathrm{e}^{\mathrm{i}\tilde{\phi}_{12}} + \tilde{\sigma}_3^{\dagger}\tilde{\sigma}_1\,\mathrm{e}^{\mathrm{i}\tilde{\phi}_{31}} + \tilde{\sigma}_2^{\dagger}\tilde{\sigma}_4\,\mathrm{e}^{\mathrm{i}\tilde{\phi}_{24}}\right. \\ &\quad \left. + \tilde{\sigma}_4^{\dagger}\tilde{\sigma}_3\,\mathrm{e}^{\mathrm{i}\tilde{\phi}_{43}} + \tilde{\sigma}_2^{\dagger}\tilde{\sigma}_3\,\mathrm{e}^{\mathrm{i}\tilde{\phi}_{23}}\right) + \mathrm{h.c.}, \end{aligned} \tag{2}$$

where the phases $\tilde{\phi}_{jk}$ can be expressed as $\tilde{\phi}_{jk} = \phi_{jk} - \phi_j + \phi_k$. As a result, the total phases in each triangular plaquette are gauge-invariant, which thus we can refer to as the flux penetrating the triangular plaquette in the same way as a magnetic field emerges,

$$\begin{aligned} \tilde{\phi}_{12} + \tilde{\phi}_{23} + \tilde{\phi}_{31} &= \phi_{12} + \phi_{23} + \phi_{31} = \Phi_1, \\ \tilde{\phi}_{24} + \tilde{\phi}_{43} + \tilde{\phi}_{32} &= \phi_{24} + \phi_{43} + \phi_{32} = \Phi_2. \end{aligned} \tag{3}$$

The gauge-invariant phase may break the time-reversal symmetry as we already know from the integer quantum Hall effect (IQHE), which manifests the chiral edge states in the presence of a magnetic field.[21,22] According to the conclusion of Ref. [23], the time-reversal symmetry is preserved if and only if the gauge-invariant phase is an integer multiple of π for any loop. As a consequence, the most significant instance of broken time-reversal symmetry occurs when the gauge-invariant phase is exactly the midway between the time-reversal symmetric points, i.e., $\pm\pi/2\,(\mathrm{mod}2\pi)$, which is just the scenario we are interested in. In the model we consider here, we focus on the case in which the two triangular plaquettes are penetrated by opposite magnetic fluxes that are both equal to $\pi/2$ in magnitude, that is $\Phi_1 = -\Phi_2 = \Phi$ and $\Phi = \pm\pi/2$. Under this condition, while the globe flux is zero, the local flux in each triangular lattice is not. Hence the time-reversal symmetry of the system is still broken.

As shown in Fig. 1(b), the model we examine is equivalent to the one-dimensional chain of next-nearest neighbor (NNN) coupling. In many-body physics, a one-dimensional chain composed of spin 1/2 particles can be mapped to a one-dimensional spinless fermionic system by the Jordan–Wigner transformation in which an individual spin-up or spin-down state can be equivalently described by occupied or unoccupied fermionic states. According to the result of Ref. [24], in addition to the trivial two-body transition terms, the equivalent spinless Fermion system Hamiltonian also includes nontrivial four-body interaction terms such as $a_1^{\dagger}a_3a_2^{\dagger}a_2$, $a_2^{\dagger}a_4a_3^{\dagger}a_3$, etc. under the Jordan–Wigner transformation.

We now consider the dynamic evolution of the spin systems. First, we notice that the Hamiltonian commutes with the total excitation operator or the total spin operator in the z-direction, i.e., $\left[H, \sum_{j=1}^{4}\sigma_j^{\dagger}\sigma_j\right] = \left[H, \sum_{j=1}^{4}S_j^z\right] = 0$. Therefore, the total excitation of the spin systems is conserved, and the Hilbert space can be divided into subspaces with different total excitations. For the sake of simplicity, under a proper gauge transformation, we consider the Hamiltonian

$$H = g\left(\sigma_1^{\dagger}\sigma_2 + \sigma_3^{\dagger}\sigma_1 + \sigma_2^{\dagger}\sigma_4 + \sigma_4^{\dagger}\sigma_3 + \mathrm{e}^{\mathrm{i}\Phi}\sigma_2^{\dagger}\sigma_3\right) + \mathrm{h.c.}, \tag{4}$$

where $\Phi = \pm\pi/2$ as mentioned above, and concentrate on the one excitation subspace (1ES), which is composed of $\{|1000\rangle, |0100\rangle, |0010\rangle, |0001\rangle\}$. The eigenvalues of the Hamiltonian are 0, 0 and $\pm\sqrt{5}g$ constrained to the 1ES subspace, which means the energy spectrum of the system in the 1ES is mirror-symmetric about the zero energy and is two-fold degenerate at the zero energy. It is straightforward to see that the Hamiltonian exhibits a permutation symmetry described by the permutation operator $P_{4231} = (I + \boldsymbol{\sigma}_1 \cdot \boldsymbol{\sigma}_4)/2$ which exchanges the states of particle 1 and particle 4. With the permutation operator and the Hamiltonian as the complete set of commuting observations (CSCO), we can lift the degeneracy and derive the dynamics of the system analytically. If the initial state is $|1000\rangle$, the spin transport dynamics of the system

for $\Phi = \pm\pi/2$ is

$$
\begin{aligned}
P_{1000}(t) &= \left[\frac{3}{5} + \frac{2}{5}\cos\left(\sqrt{5}gt\right)\right]^2, \\
P_{0100}(t) &= \left[\frac{1}{5} + \frac{\sqrt{6}}{5}\cos\left(\sqrt{5}gt \pm \phi_1\right)\right]^2, \\
P_{0010}(t) &= \left[\frac{1}{5} + \frac{\sqrt{6}}{5}\cos\left(\sqrt{5}gt \mp \phi_1\right)\right]^2, \\
P_{0001}(t) &= \left[\frac{2}{5} + \frac{2}{5}\cos\left(\sqrt{5}gt - \pi\right)\right]^2,
\end{aligned} \tag{5}
$$

where the phase $\phi_1 = \tan^{-1}(\sqrt{5})$ is in the third quadrant. The above results indicate that when $\Phi = +\pi/2$, the spin transport follows the direction $1 \Longrightarrow 2 \Longrightarrow 4 \Longrightarrow 3 \Longrightarrow 1$. However, when $\Phi = -\pi/2$, the spin transport follows the direction $1 \Longrightarrow 3 \Longrightarrow 4 \Longrightarrow 2 \Longrightarrow 1$. Similarly, if the initial state is $|0100\rangle$, the spin transport dynamics of the system for $\Phi = \pm\pi/2$ is

$$
\begin{aligned}
P_{1000}(t) = P_{0001}(t) &= \left[\frac{1}{5} + \frac{\sqrt{6}}{5}\cos\left(\frac{\sqrt{5}}{2}\Omega t \mp \phi_1\right)\right]^2, \\
P_{0100}(t) &= \left[\frac{2}{5} + \frac{3}{5}\cos\left(\frac{\sqrt{5}}{2}\Omega t\right)\right]^2, \\
P_{0010}(t) &= \left[\frac{2}{5} + \frac{3}{5}\cos\left(\frac{\sqrt{5}}{2}\Omega t \pm \phi_2\right)\right]^2,
\end{aligned} \tag{6}
$$

where the phase $\phi_2 = \tan^{-1}(\sqrt{5}/2)$ is in the third quadrant. The above results indicate that when $\Phi = +\pi/2$, the spin transport follows the direction $2 \Longrightarrow 3 \Longrightarrow 1,4 \Longrightarrow 2$. However, when $\Phi = -\pi/2$, the spin transport follows the direction $2 \Longrightarrow 1,4 \Longrightarrow 3 \Longrightarrow 2$. In summary, the spin transport is chiral, which is a consequence of the time-reversal symmetry breaking.

3. Experimental scheme

We propose a simple scheme to implement the coupling geometry in the model based on the transverse field driving and XY-type interactions in the two-qubit computational basis subspace. More specifically, Fig. 2(a) shows an optical photograph of the two-qubit superconducting quantum processor used in the experiment. Each qubit is equipped with the X/Y line to couple with the applied transverse field drive, while the energy level is tuned through the Z line. At the same time, the XY-type interactions between the two qubits are either on or off, depending on the settings of the tunable coupler. As shown in Fig. 2(b), for the purpose of realizing the coupling geometry, first of all, at the idle point, we tune the qubit frequencies into resonance through the respective Z lines and turn off the XY-type interaction between the qubits by appropriately biasing the tunable coupler. Then, at the working point, we drive the qubits simultaneously with the resonant transverse field and turn on the XY-type interaction at the same time, where we make sure that the Rabi frequencies induced by the transverse fields applied to the qubits are both exactly twice as strong as the XY-type interaction strength, meanwhile, the phase difference between the transverse fields applied to the qubits is $\pm\pi/2$. At this moment, the Hamiltonian in the lab frame can be expressed as

$$
\begin{aligned}
H = &\sum_{j=1}^{2}\frac{1}{2}\omega_j\sigma_j^z + \sum_{j=1}^{2}\Omega_j\cos(\omega_j t + \phi_j)\left(\sigma_j^\dagger + \sigma_j\right) \\
&+ g_{12}\left(\sigma_1^\dagger\sigma_2 + \sigma_2\sigma_1^\dagger\right),
\end{aligned} \tag{7}
$$

where $\omega_1 = \omega_2$, $\Omega_1 = \Omega_2 = 2g_{12} = \Omega$ and $\phi_1 - \phi_2 = \pm\pi/2$ as stated above. In the rotating frame, the Hamiltonian can be written as

$$
\begin{aligned}
H &= \frac{\Omega}{2}\left(\sum_{j=1}^{2}\exp(\mathrm{i}\phi_j)\,\sigma_j + \sigma_1^\dagger\sigma_2 + \mathrm{h.c.}\right) \\
&= \frac{\Omega}{2}\begin{pmatrix}
0 & \exp(\mathrm{i}\phi_1) & \exp(\mathrm{i}\phi_2) & 0 \\
\exp(-\mathrm{i}\phi_1) & 0 & 1 & \exp(\mathrm{i}\phi_2) \\
\exp(-\mathrm{i}\phi_2) & 1 & 0 & \exp(\mathrm{i}\phi_1) \\
0 & \exp(-\mathrm{i}\phi_2) & \exp(-\mathrm{i}\phi_1) & 0
\end{pmatrix}.
\end{aligned} \tag{8}
$$

The Hamiltonian describes the same dynamic evolution as the model in 1ES if we map the computational basis subspace $\{|00\rangle, |01\rangle, |10\rangle, |11\rangle\}$ to the 1ES $\{|1000\rangle, |0100\rangle, |0010\rangle, |0001\rangle\}$, indicating that our scheme successfully implements the simulation of the physical model in 1ES, as depicted in Fig. 2(c).

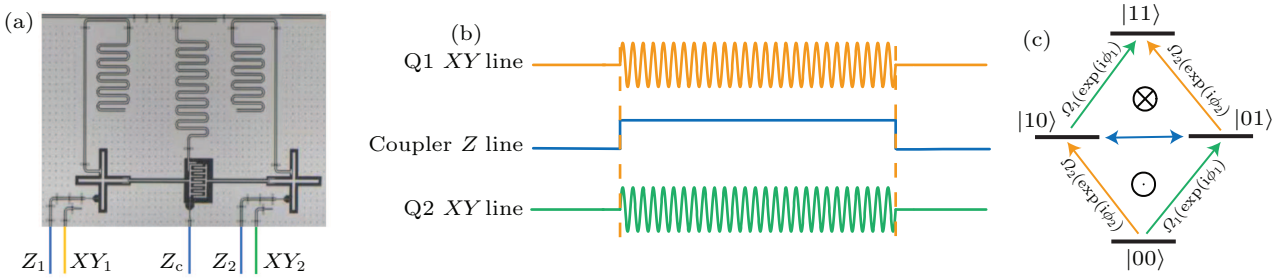


Fig. 2. The experimental scheme to simulate the physical model. (a) The optical photograph of the two-qubit superconducting quantum processor. (b) The pulse sequences that are used for generating the coupling geometry, where both the transverse fields drive the qubits simultaneously while the XY-type coupling is turned on. (c) Equivalent coupling geometry in the computational basis subspace of two qubits.

4. Experimental demonstration

We experimentally demonstrate the chiral spin states predicted by the physical model discussed above following the scheme we suggest. In our scheme, to observe the chiral dynamics in the superconducting quantum circuit, the coupling-off point needs to be carefully calibrated. To obtain this idle point, we bring both qubits into resonance with the frequency ~ 4.862 GHz, where the measured energy relaxation times of the qubits are 20 μs and 18 μs at the specific frequency bias point. And the anharmonicity of the qubits is -195 MHz and -197 MHz, respectively. The vacuum Rabi oscillation allows us to determine the coupling-off point by measuring the XY-type coupling strength between the qubits while varying the bias point of the tunable coupler.

In the multi-qubit superconducting circuit, the classical crosstalk, such as DC crosstalk, AC crosstalk or drive crosstalk, has to be calibrated and completely canceled out for precise quantum state manipulation.[25–28] Our scheme realizes the gauge-invariant phases using the transverse field drives, in contrast to parametric modulation methods, which can substantially avoid the effects of AC crosstalk. Therefore, we first extract a crosstalk matrix to eliminate the DC crosstalk with a series of specific experiments, while the drive crosstalk can be compensated by additionally applying an out-of-phase microwave drive. Further, we design a subtle calibration experiment to synchronize the phases of the traverse fields applied to each of the two qubits and ensure that the Rabi frequencies of the transverse fields are equal, while verifying that the drive crosstalk is cancelled out. The details of the experiment are shown in Appendix A.

After all these calibration works, we simultaneously apply the calibrated transverse field drives to the qubits through the XY lines and bias the tunable coupler to a specific operating point through the Z line at the same time, where the XY-type coupling strength between the qubits is exactly half of the Rabi frequency, i.e., 5.5 MHz. By using Ramsey interference, we are able to find that the ZZ-type coupling strength between the qubits is only on the order of 100 kHz at the working point,[29] which is weak enough to ensure no significant impact on our experiment. Eventually, we may examine the chiral spin currents by measuring the population dynamics of the states $|00\rangle, |01\rangle, |10\rangle, |11\rangle$ with the single-shot readout,[30–32] whose fidelities for each state are 79%, 75%, 72%, 71%, respectively. Figures 3(a), 3(b) and 4(a), 4(b) show the experiment results, where we set the gauge-invariant phase $\Phi = \pm\pi/2$ while initialize the qubits to the state $|00\rangle$ by energy relaxation and the state $|01\rangle$ by π-pulse, respectively. The population dynamics exhibit the remarkably chiral character that is determined by the local flux penetrating each triangular lattice, as predicted by the theory. The small deviation from the experiment and the theory can be attributed to the calibration accuracy of the square wave distortion and XY-type coupling strength.

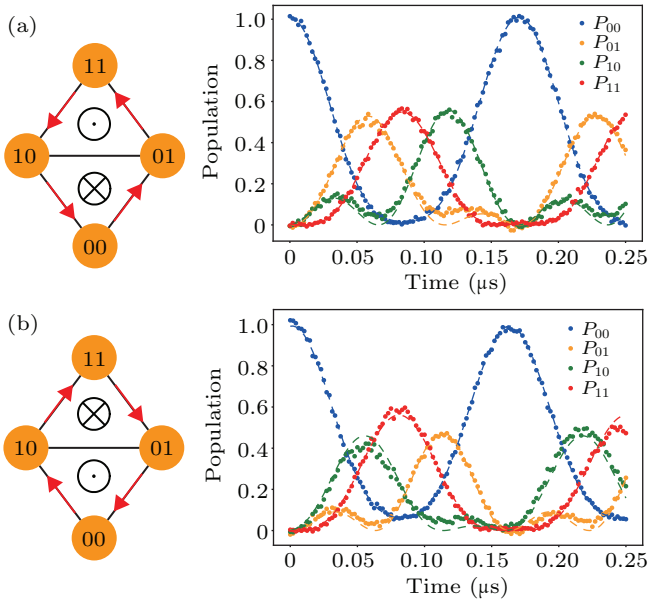


Fig. 3. The chiral dynamics when the two qubits are initialized to state $|00\rangle$. The experimental results (discrete points) and the theoretical expectations (dashed lines) are in good agreement. (a) When $\Phi = +\pi/2$, the population transport follows the direction $|00\rangle \Longrightarrow |01\rangle \Longrightarrow |11\rangle \Longrightarrow |10\rangle \Longrightarrow |00\rangle$. (b) When $\Phi = -\pi/2$, the population transport follows the direction $|00\rangle \Longrightarrow |10\rangle \Longrightarrow |11\rangle \Longrightarrow |01\rangle \Longrightarrow |00\rangle$.

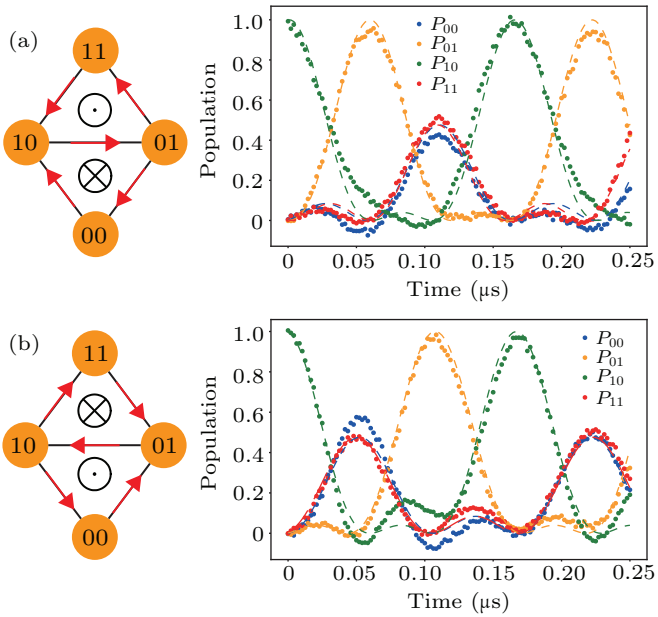


Fig. 4. The chiral dynamics when the two qubits are initialized to state $|10\rangle$. The experimental results (discrete points) and the theoretical expectations (dashed lines) are in good agreement. (a) When $\Phi = +\pi/2$, the population transport follows the direction $|10\rangle \Longrightarrow |01\rangle \Longrightarrow |00\rangle$, $|11\rangle \Longrightarrow |10\rangle$. (b) When $\Phi = -\pi/2$, the population transport follows the direction $|10\rangle \Longrightarrow |00\rangle$, $|11\rangle \Longrightarrow |01\rangle \Longrightarrow |10\rangle$.

5. Conclusion

We have investigated the dynamics of a TRSB system with non-trivial interactions and experimentally demonstrated the chiral ground spin current, which is a signature of the

TRSB. In our experimental scheme based on a two-qubit superconducting quantum processor with the tunable coupler architecture, the TRSB is realized by utilizing an effective magnetic field. Here, the field is achieved by the gauge-invariant phase in loop coupling geometries. The chiral spin current has the potential to serve for precisely calibration in the tunable coupler architecture, since the chirality is insensitive to perturbations. In the future, we can further develop the physical model to 2D coupled-chain geometries, which will manifest the gapped or gapless topological phases called chiral spin liquids (CSL) and design the multi-qubit superconducting quantum chips to simulate the highly entangled phases.[33,34]

Appendix A: Calibrate the transverse drives

As mentioned in the main text, in order to observe chiral spin current, it is essential to find a method to verify that the Rabi frequencies of the transverse fields applied to the two qubits are equal and phase-synchronous.

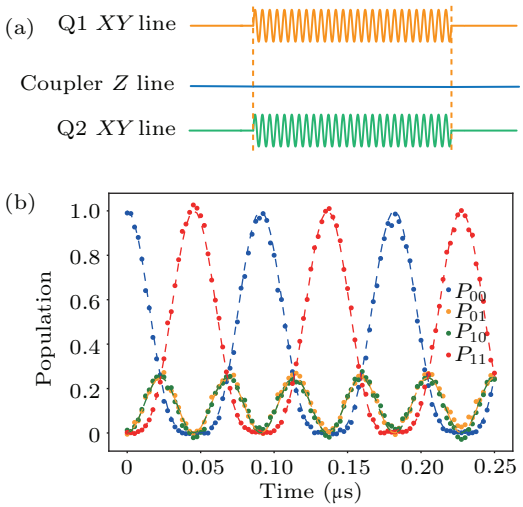


Fig. A1. The experimental scheme to calibrate the transverse field drives. (a) The pulse sequences that are used for synchronizing the transverse field drives. (b) The experimental results (discrete points) and the theoretical expectations (dashed lines) are in good agreement, which means we successfully calibrate the transverse field drives.

In the experiment, we exploit the coherence of the diamond-configuration coupling geometry to achieve this. Figure A1(a) shows the waveform sequence used for this validation experiment, we apply the transverse drives to each of the two qubits simultaneously, while the XY-type coupling is off. If the classical drive crosstalk is eliminated and the Rabi frequencies of the two transverse fields are equal in magnitude and phase-synchronous, then the Hamiltonian can be written as

$$H=\sum_{j=1}^{2}\frac{1}{2}\omega\sigma_j^z+\sum_{j=1}^{2}\Omega\cos(\omega t)\left(\sigma_j^{\dagger}+\sigma_j\right). \tag{A1}$$

If the initial state of the system is $|00\rangle$, the population dynamics is

$$\begin{aligned}P_{00}(t)&=\frac{1}{4}(1+\cos\Omega t)^2,\\ P_{11}(t)&=\frac{1}{4}(1-\cos\Omega t)^2,\\ P_{01}(t)&=P_{10}(t)=\frac{1}{4}\sin^2\Omega t.\end{aligned} \tag{A2}$$

The experimental results are shown in Fig. A1(b), which indicates that we have successfully calibrate the Rabi frequencies arising from the two transverse drives, and the magnitude of the Rabi frequency extracted from the experimental results is 11 MHz when we tune the qubits into the idler point.

Acknowledgements

Project supported by the Key R&D Program of Guangdong Province, China (Grant No. 2018B030326001), the National Natural Science Foundation of China (Grant Nos. 11474152, 12074179,U21A20436, and 61521001), and the Natural Science Foundation of Jiangsu Province, China (Grant No. BE2021015-1).

References

[1] Tsui D C, Stormer H L and Gossard A C 1982 *Phys. Rev. Lett.* **48** 1559
[2] Halperin B I 1984 *Phys. Rev. Lett.* **52** 1583
[3] Feynman R P 1982 *International Journal of Theoretical Physics* **21** 467
[4] Cirac J I and Zoller P 2012 *Nat. Phys.* **8** 264
[5] Georgescu I M, Ashhab S and Nori F 2014 *Rev. Mod. Phys.* **86** 153
[6] Manovitz T, Shapira Y, Akerman N, Stern A and Ozeri R 2020 *PRX Quantum* **1** 020303
[7] Graß T, Celi A, Pagano G and Lewenstein M 2018 *Phys. Rev. A* **97** 010302
[8] Periwal A, Cooper E S, Kunkel P, Wienand J F, Davis E J and Schleier-Smith M 2021 *Nature* **600** 630
[9] Lienhard V, Scholl P, Weber S, Barredo D, de Léséleuc S, Bai R, Lang N, Fleischhauer M, Büchler H P, Lahaye T, *et al.* 2020 *Phys. Rev. X* **10** 021031
[10] Cai W, Han J, Mei F, Xu Y, Ma Y, Li X, Wang H, Song Y, Xue Z Y, Yin Z q et al. 2019 *Phys. Rev. Lett.* **123** 080501
[11] Guo X Y, Ge Z Y, Li H, Wang Z, Zhang Y R, Song P, Xiang Z, Song X, Jin Y, Lu L, *et al.* 2021 *npj Quantum Information* **7** 1
[12] Neill C, McCourt T, Mi X, Jiang Z, Niu M, Mruczkiewicz W, Aleiner I, Arute F, Arya K, Atalaya J, *et al.* 2021 *Nature* **594** 508
[13] Barends R, Kelly J, Megrant A, Veitia A, Sank D, Jeffrey E, White T C, Mutus J, Fowler A G, Campbell B, *et al.* 2014 *Nature* **508** 500
[14] Yan F, Krantz P, Sung Y, Kjaergaard M, Campbell D L, Orlando T P, Gustavsson S and Oliver W D 2018 *Phys. Rev. Appl.* **10** 054062
[15] Li X, Cai T, Yan H, Wang Z, Pan X, Ma Y, Cai W, Han J, Hua Z, Han X, *et al.* 2020 *Phys. Rev. Appl.* **14** 024070
[16] Sete E A, Chen A Q, Manenti R, Kulshreshtha S and Poletto S 2021 *Phys. Rev. Appl.* **15** 064063
[17] Roushan P, Neill C, Megrant A, Chen Y, Babbush R, Barends R, Campbell B, Chen Z, Chiaro B, Dunsworth A, *et al.* 2017 *Nat. Phys.* **13** 146
[18] Liu W, Feng W, Ren W, Wang D W and Wang H 2020 *Appl. Phys. Lett.* **116** 114001
[19] Vepsäläinen A and Paraoanu G S 2020 *Advanced Quantum Technologies* **3** 1900121
[20] Wang D W, Song C, Feng W, Cai H, Xu D, Deng H, Li H, Zheng D, Zhu X, Wang H, *et al.* 2019 *Nat. Phys.* **15** 382
[21] Klitzing K v, Dorda G and Pepper M 1980 *Phys. Rev. Lett.* **45** 494

[22] Xiang Z C, Huang K, Zhang Y R, Liu T, Shi Y H, Deng C L, Liu T, Li H, Liang G H, Mei Z Y, *et al.* 2022 arXiv preprint arXiv:2207.11797
[23] Koch J, Houck A A, Le Hur K and Girvin S 2010 *Phys. Rev. A* **82** 043811
[24] Shapira Y, Manovitz T, Akerman N, Stern A and Ozeri R 2022 arXiv preprint arXiv:2205.11178
[25] Ash-Saki A, Alam M and Ghosh S 2020 *IEEE Transactions on Quantum Engineering* **1** 1
[26] Abrams D M, Didier N, Caldwell S A, Johnson B R and Ryan C A 2019 *Phys. Rev. Appl.* **12** 064022
[27] Mundada P, Zhang G, Hazard T and Houck A 2019 *Phys. Rev. Appl.* **12** 054023
[28] Nuerbolati W, Han Z, Chu J, Zhou Y, Tan X, Yu Y, Liu S and Yan F 2022 *Appl. Phys. Lett.* **120** 174001
[29] Stehlik J, Zajac D, Underwood D, Phung T, Blair J, Carnevale S, Klaus D, Keefe G, Carniol A, Kumph M, *et al.* 2021 *Phys. Rev. Lett.* **127** 080505
[30] Mallet F, Ong F R, Palacios-Laloy A, Nguyen F, Bertet P, Vion D and Esteve D 2009 *Nat. Phys.* **5** 791
[31] Filipp S, Maurer P, Leek P J, Baur M, Bianchetti R, Fink J, Göppl M, Steffen L, Gambetta J M, Blais A, *et al.* 2009 *Phys. Rev. Lett.* **102** 200402
[32] Dewes A, Ong F R, Schmitt V, Lauro R, Boulant N, Bertet P, Vion D and Esteve D 2012 *Phys. Rev. Lett.* **108** 057002
[33] Gorohovsky G, Pereira R G and Sela E 2015 *Phys. Rev. B* **91** 245139
[34] Buccheri F, Egger R, Pereira R G and Ramos F B 2018 *Phys. Rev. B* **97** 220402